Superparamagnetic segmentation by excitable neural systems

Juan P. Neirotti, Samuel M. Kurcbart,* and Nestor Caticha
Departamento de Física Geral, Instituto de Física, Universidade de São Paulo, Rua do Matão Travessa R 187, CEP 05508-900, São Paulo, Brazil

(Received 24 February 2003; published 23 September 2003)

Magnetic modeling for clustering or segmentation purposes can either associate the image data to external quenched fields or to the interactions among a set of auxiliary variables. The latter gives rise to superparamagnetic segmentation and is usually done with Potts systems. We have used the superparamagnetic clustering technique to segment images, with the aid of different associated systems. Results using Potts model are comparable to those obtained using excitable FitzHugh-Nagumo and Morris-Lecar model neurons. Interactions between the associated system components are a function of the difference of luminosity on a gray scale of neighbor pixels and the difference of membrane potential.

DOI: 10.1103/PhysRevE.68.031911 PACS number(s): 87.19.La, 05.10.−a, 07.05.Pj

I. INTRODUCTION

The interpretation of a dynamical system as a computer, e.g., a *machine* that accepts an input, processes it using a dynamical rule and returns an output, permits to devise computational tools based on analogies to physical systems. This strategy is intensively used in the present work. Given a set of data points in a feature space, the problem of separating or rather, organizing them into categories is a traditional one appearing in several areas in science. It comes under names such as density estimation, categorization, unsupervised learning, clustering, exploratory data analysis, or segmentation. The unsupervised characterization of points is performed by the identification of a similarity measure of groups, typically pairs, of points. Above a given threshold, the group is assigned to the same cluster. Two clusters having a point in common, form a single cluster. Thus, two clusters are different only if they have no points in common. The measure should have several properties, but above all, it must permit robust categorization. *Ad hoc* changes of the threshold criteria, at least within a given interval, should have small changes in the classification. Depending on the amount of prior information, different methods can be acceptable.

A very important idea has been put forward by Domany and co-workers [1]. They defined the similarity measure based on the collective properties of an ancillary magnetic system. To each data point, a q-state Potts magnetic spin is associated [2]. Two-body ferromagnetic spin interactions are defined—but antiferromagnetic extensions or, e.g., three-body interactions are possible—as a monotonically decreasing function of the Euclidean distance (which is not a robust similarity measure by itself). Different collective behavior can arise as a function of the temperature of the ancillary system. It is natural to use the spin-spin correlation function as a similarity measure. While phase transitions are only possible in the thermodynamic limit, for sufficiently large number of data points, numerically clear transitions can be seen. At high temperatures the system is in the paramagnetic (disordered) phase, and each spin is itself a cluster. At very low temperatures almost all the spins belong to the same cluster (ferromagnetic phase). At intermediate temperatures *superparamagnetic* phases can be found, at which independent spin domains appear. A cluster is formed by the data points associated to the spins in a given category. Other ancillary choices can be made. A trivial change is done by looking at other values of q. This has, within broad limits, no influence in the resulting categorization. Note that the number of categories is not determined by q. Other spin models can be used, such as $Z(q)$ or clock models.

The question we address in this paper is whether biologically inspired models of neurons can be used in place of magnetic variables. This bears on the question whether superparamagneticlike segmentation can occur by the dynamics of the visual system. Instead of associating a spin to each data point, we associate a nonlinear oscillator inspired in electrical models of neuronal membranes derived from the Hodgkin and Huxley model. One of the results of this paper is, as is often stated in the literature [3], that we find that the collective dynamical behavior of the coupled oscillators can also serve to form categories. We have used the FitzHugh-Nagumo and Morris-Lecar neurons. Both types have been used to describe the behavior of the action potential in different kinds of nervous cells. They respond to an input current that, in the present case, is a sum of contributions from neighbors plus an external input current. These contributions are mediated by interactions analogous to the exchange interactions in the Potts model and biologically can be thought as implemented through the action of interneurons. Strongly coupled oscillators will tend to have correlated membrane potentials while uncoupled neighbors will likely oscillate independently, but whether potentials are correlated or not will ultimately be a collective property. Therefore, the correlation can be used as a similarity measure as was the case for Potts variables. We will show that the mean value of the oscillator frequency over the population has an equivalent role to that of the magnetization in the spin system and the external input current plays the part of the temperature. Thus it is possible to find an interval of external input currents in which a

*Permanent address: Departamento de Ciências Naturais, Universidade Federal de São João do Rei, CEP 36301-160 São João do Rei, MG. Brazil.

superparamagnetic phase occurs in the neural oscillators.

Temporal synchronization of locally coupled oscillators have already been used to segment images. In Ref. [4], a locally excitatory globally inhibitory oscillator network (LEGION) was used [5], each oscillator coupled with its local neighbors and with a global inhibitor. The input current used was different for stimulated and not stimulated oscillators, and the couplings were ruled by a dynamic law. In Refs. [6,7], the amplitude and frequency of the oscillators were used to separate observed objects from background. The oscillators used herein were of the FitzHugh-Nagumo type, connected by couplings that depended on the difference of the membrane potential between neighbors with an input current for each oscillator depending on the gray level of the correspondent pixel. To desynchronize clusters corresponding to neighbor objects with the same intensity in the input image, an attention driven mechanism was introduced. The mechanism was implemented by a saliency map, with elements that had an activity defined in such a way to mimic the functionality of real neural structures. Although our approach is apparently similar to the described (LEGION oscillators even look like FitzHugh-Nagumo oscillators), we stimulate all the oscillators in the network with the same input current. The oscillators are coupled by a static hardwired connection that obeys a Gaussian law with the distance (see below), modulated by a dynamic factor that depends on the difference of the membrane potential between neighbors. This factor is zero when neighboring oscillators are in synchrony or when the static connection is negligible. The time correlation function among neighbors is then measured with the aim to use it as a similarity measure. Our approach is much simpler, given that there are just two dynamic variables per oscillator and there is no nead for a desynchronization mechanism.

Since there is no *a priori* rule to categorize the subgroups, nor any knowledge about the number of subgroups, there are no criteria to verify which solution is the *best*. The success of a clustering mechanism should be measured in a problem-dependent (specialized) way. A *specialist* is frequently called upon to determine an acceptable solution. From that a merit figure can be attributed to each segmentation. We construct a specialist image by segmentation of an image by hand. This is used to measure merit figures for all systems, which come out as comparable.

In Sec. II we present the three models used for segmentation, the two biological models and the Potts based model. The results of Monte Carlo (MC) simulations and integration of the systems of coupled ordinary differential equations are presented in Sec. III. Section IV presents the conclusions.

II. THE MODELS

The superparamagnetic clustering method, irrespective of whether it is based on magnetic variables such as Potts spins or artificial neurons, starts by determining a set of numbers which describe the interactions among pairs of dynamical units. This is based on information $\{(x_n,y_n,z_n)\}$ about the image. For each pixel n of coordinates (x_n,y_n) an integer z_n is given, which measures its luminosity or gray level (e.g., $0 \leqslant z_n \leqslant 255$). The image can thus be represented by a a set of points in a three-dimensional space, each at a position

$$\mathbf{r}_n = x_n\mathbf{i} + y_n\mathbf{j} + \alpha z_n\mathbf{k}, \tag{1}$$

where α is a suitable scale constant, and **i**, **j**, and **k** are the orthonormal vectors of the three-dimensional space. The interaction $J_{ij}=J(d_{ij})$ is a decreasing function of the distance $d_{ij}=|\mathbf{r}_i-\mathbf{r}_j|$ between pixels i and j, which is not, in general, itself a robust criterion for categorization. The sum is over a set of sites in which we choose to include first and possibly second nearest neighbors. Local interactions can be defined in several ways, and here we will restrict to ferromagnetic or excitatory interactions. It is usual to define (as the permanent connection weights in the LEGION system [4])

$$J_{ij} = \frac{1}{\hat{K}} \exp\left(-\frac{d_{ij}^2}{2a^2} \right), \tag{2}$$

where $\hat{K}$ is the number of neighbors considered (4 or 8, first-nearest or first- and second-nearest neighbors) and a is a scale constant. α and a are free parameters that have to be adjusted.

A. Potts model

The Potts model Hamiltonian is given by

$$H = -\sum_{(i,j)} J_{ij}\delta_{s_i s_j}, \tag{3}$$

where $s_i = 1,2,\ldots,q$, $\delta_{s_i s_j}$ is the Kronecker delta symbol ($\delta_{s_i s_j}=1$ if $s_i=s_j$, and zero otherwise) and (i,j) represents the set of sites j that are in the neighborhood of the site i. The order parameter of the system is the mean magnetization $\langle m \rangle$,

$$\langle m \rangle = \frac{q\langle N_{max}/N \rangle - 1}{q-1}, \tag{4}$$

where $N_{max}=\max\{N_1,N_2,\ldots,N_q\}$, N_μ is the number of sites of a configuration in state μ, and N is the total number of sites. To localize the superparamagnetic region of parameters the usual response function is the susceptibility χ,

$$\chi = \frac{N}{T}\langle (m - \langle m \rangle)^2 \rangle. \tag{5}$$

In order to define the clustering criteria we have to numerically determine the spin-spin correlation function $\langle \delta_{s_i s_j} \rangle$. The Swendsen and Wang (SW) algorithm [8] is a common choice for simulating these systems. An improvement that leads to a faster convergence of the quantities used in the segmentation process is given by the energy-based cluster update (ECU) algorithm, [9,10]. In terms of the SW bond variables n_{ij} between spins i and j, the correlation function is given by

$$\langle \delta_{s_i s_j} \rangle = \frac{(q-1)\langle n_{ij} \rangle + 1}{q}. \tag{6}$$

Bond clusters are not the answer for the clustering problem. Bond clusters are dynamical objects, while spin clusters are objects defined in thermodynamic equilibrium.

B. FitzHugh-Nagumo and Morris-Lecar models

The landmark in modeling action potential and related membrane phenomena, the work of Hodgkin and Huxley (HH) [11], gave rise to several variants. Such generalizations may include either more elements of biological realism or result from simplifications, which at the expense of realism, lead to more manageable mathematical models. They modeled the total membrane current by a sum of two contributions, an ionic plus a capacitive current. Ionic currents are due to the ionic flux through the membrane channels. The model captures the dynamic behavior in four equations for each neuron compartment: one for the membrane potential and three for the state variables determining the state of the ionic channels. For a general exposition about such models, see, e.g., the work by Koch [12].

The simplifications start by noting that there are at least two separate time scales in the HH model. The membrane potential and the sodium activation variable in the HH model evolve on similar time scales, while the other two state variables, potassium activation and sodium inactivation, evolve on a similar, albeit much slower time scale. Given that the time dependency of the first pair of variables is very similar, a single dynamic variable $V(t)$ is used to represent them collectively. In the same way, the slow variables in the HH model are replaced by one slow variable, $W(t)$. In this manner, using the phase space method in the context of a chemical reaction bearing some similarities to nerve cell excitation, FitzHugh [13] and, independently, Nagumo, Arimoto, and Yoshizawa [14] derived the following two equations to qualitatively describe the events occurring in an excitable neuron:

$$\varepsilon\frac{dV}{dt}=f(V)-W+I_{\mathrm{ext}},$$

$$\frac{dW}{dt}=V-pW-b. \tag{7}$$

$f(V)$ introduces the nonlinearity and is given by $f(V)=V(V-a)(1-V)$. The excitable behavior of the FitzHugh-Nagumo (FHN) system is quite robust. The single FHN neuron will go to a spiking limit cycle for $I_{-}<I_{\mathrm{ext}}<I_{+}$, where $I_{\pm}=(V_{\pm}-b)/p-f(V_{\pm})$ and $V_{\pm}$ are the extrema of f. The values of the parameters, in no way critical where chosen as follows: ε, which sets the ratio of time scales was taken as $\varepsilon=0.005$; a, b, and p are positive dimensionless constants and the values we use are $a=0.5$, $b=0.15$, and $p=1$. I_{ext} is an external input current which for the coupled system will incorporate the bias plus the influence of neighboring units. For this choice of parameters, if $0.109<I_{\mathrm{ext}}<0.591$ the spikes appear. Outside this range, the system goes to a stable point. At these limits the system undergoes a Hopf bifurcation and therefore the frequency jumps discontinuously. To compare with a system which presents a continuous onset of spiking, we looked also at the Morris-Lecar model.

The system of coupled equations presented by Morris and Lecar [15] to model barnacle muscle fibers develops a saddle bifurcation for the parameters we choose [16] and thus can present arbitrarily small frequencies, and is given by

$$C_m\frac{dV}{dt}=-I_{\mathrm{ionic}}(V,W)+I_{\mathrm{ext}},$$

$$\frac{dW}{dt}=\frac{W_\infty(V)-W}{\tau(V)}, \tag{8}$$

where V is the membrane potential (in millivolts), $C_m=1\ \mu\mathrm{F/cm}^2$, and W is the activation variable for potassium channels. All currents are in units of $\mu\mathrm{A/cm}^2$ and time t is measured in milliseconds. The ionic current has three components,

$$I_{\mathrm{ionic}}(V,W)=G_{\mathrm{Ca}}m_\infty(V)(V-E_{\mathrm{Ca}})+G_{\mathrm{K}}W(V-E_{\mathrm{K}})+G_m(V-V_{\mathrm{rest}}).$$

We assume that the calcium conductance is always at equilibrium, with its activation curve given by

$$m_\infty(V)=\frac{1}{2}\left(1+\tanh\frac{V+1}{15}\right).$$

The potassium activation variable obeys the following activation law:

$$W_\infty(V)=\frac{1}{2}\left(1+\tanh\frac{V-10}{14.5}\right),$$

and time constant

$$\tau(V)=3\ \ \mathrm{sech}\frac{V-10}{29}.$$

The value of the parameters are $G_{\mathrm{Ca}}=1$, $G_{\mathrm{K}}=2$, $G_m=0.5$, $E_{\mathrm{Ca}}=100$, $E_{\mathrm{K}}=-70$, and $V_{\mathrm{rest}}=-50$. All conductances are in units of $\mathrm{mS/cm}^2$ and the reversal potentials in millivolts. At $I=8.326$ the isolated Morris-Lecar (ML) neuron starts spiking with arbitrarily small frequency (saddle bifurcation).

For both types of neurons, as in the usual Potts case, we associate to each pixel a single-compartment neuron. Each one interacts with its neighbors by a fast coupling, which can be attributed to horizontal interneurons, which are afferent from the sensory cells. In addition, a constant input current stimulates each unit:

$$I_i=I\left[\lambda_0+\lambda_1\sum_j J_{ij}(V_j-V_i)\right], \tag{9}$$

where I sets in the overall scale of the current, playing a similar role to that of the temperature in the spin system, λ_0 and λ_1 are noncritical free parameters that have to be adjusted, J_{ij} is the coupling constant between oscillators and it is given by Eq. (2) and the sum runs over all sites j that are first neighbors to i. When the ith oscillator is not synchronized with its neighbors, the second term in Eq. (9) is zero

only if $J_{ij}=0$. Thus, if $J_{ij}\neq 0$ and if $I\lambda_0$ is within the range of currents at which the oscillations are developed, the second contribution pushes the value of I_i out of this regime and the dynamic variables go to the stable point. The stable point is common for all oscillators that receive the same input current, thus, from this stable point as a new initial condition, strongly coupled oscillators start in synchrony a new burst of oscillations. When the oscillators are synchronized, $\lambda_1 \Sigma_j J_{ij}(V_j - V_i)$ is zero, so the oscillators keep spiking indefinitely. If $J_{ij}=0$ there is no mechanism to synchronize the oscillators, so their synchrony depends on the (random) initial conditions.

The order parameter, equivalent to the magnetization in the spin systems, is the mean oscillators frequency,

$$\langle f \rangle = \frac{1}{N} \sum_i f_i ,$$

where f_i is the frequency of the spikes at pixel i. The sum runs over all the pixels in the figure. This quantity will serve to characterize the superparamagnetic regime.

The simulation starts with all the oscillators having random initial configurations. The equations for W, which are very simple and uncoupled, were integrated using the Euler exponential method, see Ref. [17] for an exposition of the method. The equations for V, which are coupled by the external current term, were integrated with a semi-implicit method. In order to perform the clustering, the correlation

$$\overline{\rho_{ij}} = \frac{\sum_{k=1}^{N_S} [V_i(k\delta t) - \overline{V_i}][V_j(k\delta t) - \overline{V_j}]}{\sqrt{\left[\sum_{k=1}^{N_S} [V_i(k\delta t) - \overline{V_i}]^2\right]\left[\sum_{k=1}^{N_S} [V_j(k\delta t) - \overline{V_j}]^2\right]}}, \tag{10}$$

was measured. Here δt is the time step in the numerical integration, N_S is the number of numerical integration steps, and the horizontal bar indicates time average. Equation (10) plays the same role as Eq. (6). The numerical integration was tested and compared on short runs with a much slower fourth-order Runge-Kutta method to verify the integration programs. Discarded initial transients and integration times are discussed below. The correlation of W variables, induced via the membrane potentials, can also be used as a clustering criterion leading to identical results.

III. IMAGE SEGMENTATION

The method consists of two steps: First, the recognition of the control parameter range (temperature for the spin system and external current for the oscillator system) at which the superparamagnetic regime is developed. Second, for the values of the control parameter in this interval, the correlations [Eqs. (6) and (10) for the spin and oscillator systems, respectively] are calculated in order to perform the image segmentation.

The superparamagnetic regime is characterized by a *plateau* in the order parameter curve. For values of the control parameter at which the *plateau* is developed, the correlations are calculated and compared with a similarity threshold θ. If the correlation between two pixels is larger than θ, the pixels are similar, and both belong to the same cluster. Each dynamical variable cluster is identified with a figure segment at the end of the simulation.

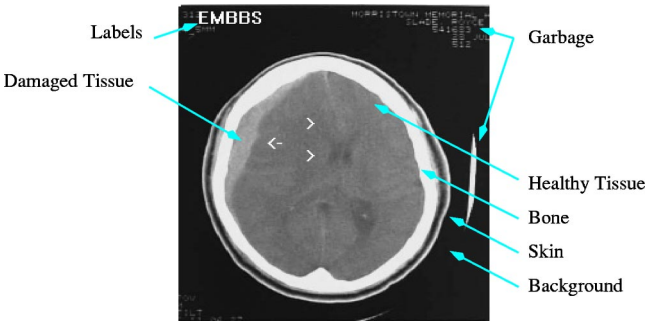

FIG. 1. X-ray computerized tomography image of a damaged human brain. It presents five regions that can be visualized with ease: the dark background, a thin structure (skin) surrounding a bright ring (bone), a gray structure inside the ring (brain), and a light gray structure between the brain and the bone at the top left (damaged tissue). Labels and other structures (arrows, the bright strip at the right of the figure or the tiny bright structures at the top right) are not interesting for segmentation purposes.

A. Example

We have used the image shown in Fig. 1 as an application example. This image has 240×256 pixels, and gray scale (0–255). We performed a SW Monte Carlo with the parameters shown in Table I and integrations of the equation systems (7) and (8) with parameters shown in Table II.

Let us first study the spin system results. At high temperatures the system is in the disordered phase. During the simulated annealing (diminishing the temperature) the lattice spins start to see each other. At low temperatures the system is in an ordered (ferromagnetic) phase. There is an intermediate temperature region at which we get the best images. A long simulation has been performed in order to get a benchmark magnetization curve. Using a first-nearest-neighbor algorithm ($\hat{K}=4$), the magnetization and susceptibility curves obtained for 50 temperatures in the range $0.001 \leqslant k_B T/\varepsilon$

TABLE I. Parameter values for the SW Monte Carlo simulation.

Parameters	Values
$\hat{K}$	4
a	10
α	2.5
q	12
$k_B T_{max}/\varepsilon$	0.18
$k_B T_{min}/\varepsilon$	0.001
θ	0.5
NT	50
MCPs	20 000

TABLE II. Parameter values for the integration of systems (7) and (8). In both cases the warm-up time was $N_S/5$.

Parameters	FHN values	ML values
$\hat{K}$	4	4
a	10	10
α	5	5
$\lambda_0/\hat{K}$	0.3	0.3
λ_1	1.2	1.2
N_s	500	1000
I_{max}	1.0	30.0
I_{min}	0.0	5.0
θ	0.5	0.5
δt	0.01	0.04

$\leqslant 0.18$, after 20 000 MC passes (each MC pass represents an update of the entire spin configuration), separated in 10 independent trials, are presented in Fig. 2. The total time needed to get these curves in a 300-MHz, Pentium II PC was 5 h, 20 min.

There is a *plateau* in the magnetization curve, associated with the superparamagnetic phase. In this interval of temperatures, the system develops spin domains that can be associated with image segments. In Fig. 3 we have presented a set of images obtained at the temperatures marked with a ● in Fig. 2. It is important to note that the best pictures from this set (using the bare eye as specialist) appear when the system is in the superparamagnetic phase. If the temperature

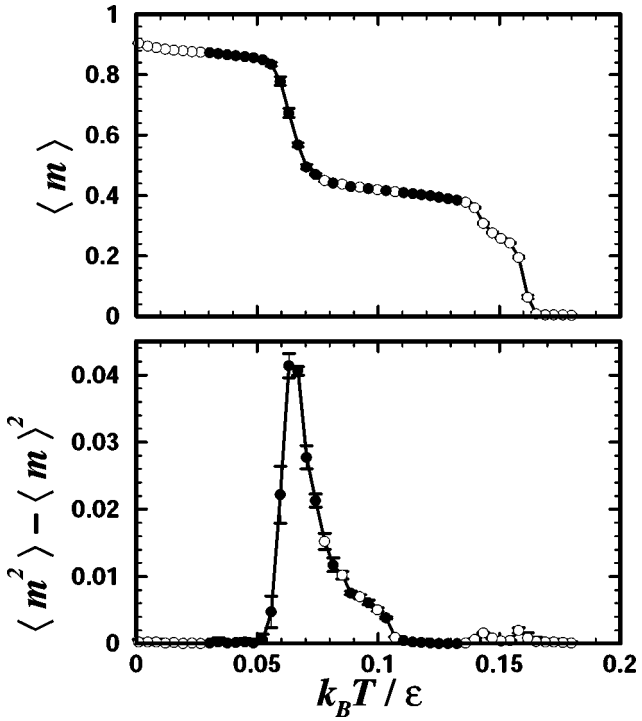

FIG. 2. Magnetization (top) and fluctuations (bottom) of the magnetization for the spin system associated to Fig. 1. The ○ mark the data points and the ● mark the temperatures at which the images of Fig. 3 were taken.

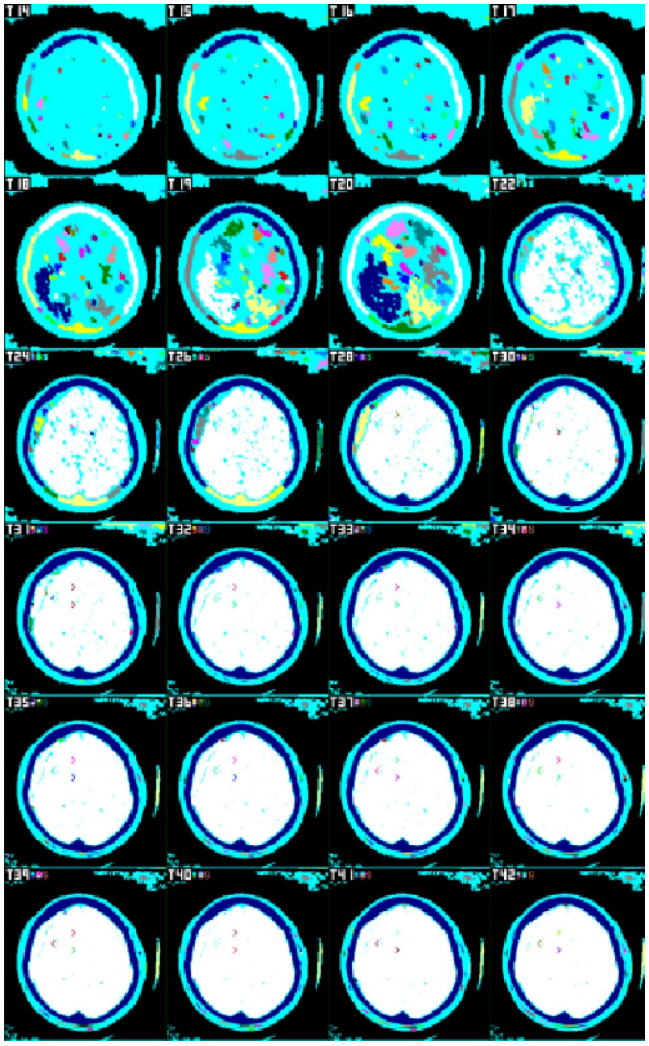

FIG. 3. Segmentation of the original image presented in Fig. 1, using the Potts spin model clustering, for the temperatures marked with ● in Fig. 2.

is too high (first images) the image is too noisy; whereas at too low temperatures (last images) the image presents just a few segments and details are lost.

Because we are looking only for the 40 biggest segments in each figure, the segmentation figures present light gray (cyan, for the on-line version of the paper) regions that are single pixels or pixel clusters with areas smaller than the smallest segment considered. We will refer to this regions as noise.

For the FitzHugh-Nagumo oscillator system, the external currents are fixed at the interval $0<I_{\text{ext}}<1$. At currents above 0.6 and below 0.1 the system is disordered and oscillators are mainly independent. We can characterize this region as a paramagnetic phase. When the current is raised above 0.1, the system enters a ferromagneticlike regime. The ferromagnetic phase ends at an external current of about 0.5. For values above 0.5 and below 0.6, there is a superparamagneticlike phase. In this region we obtained the best images, similar in quality to those obtained at the superparamagnetic regime in the spin system. The time for a simulation of 100 plus 500 integration steps at 50 different values of the exter-

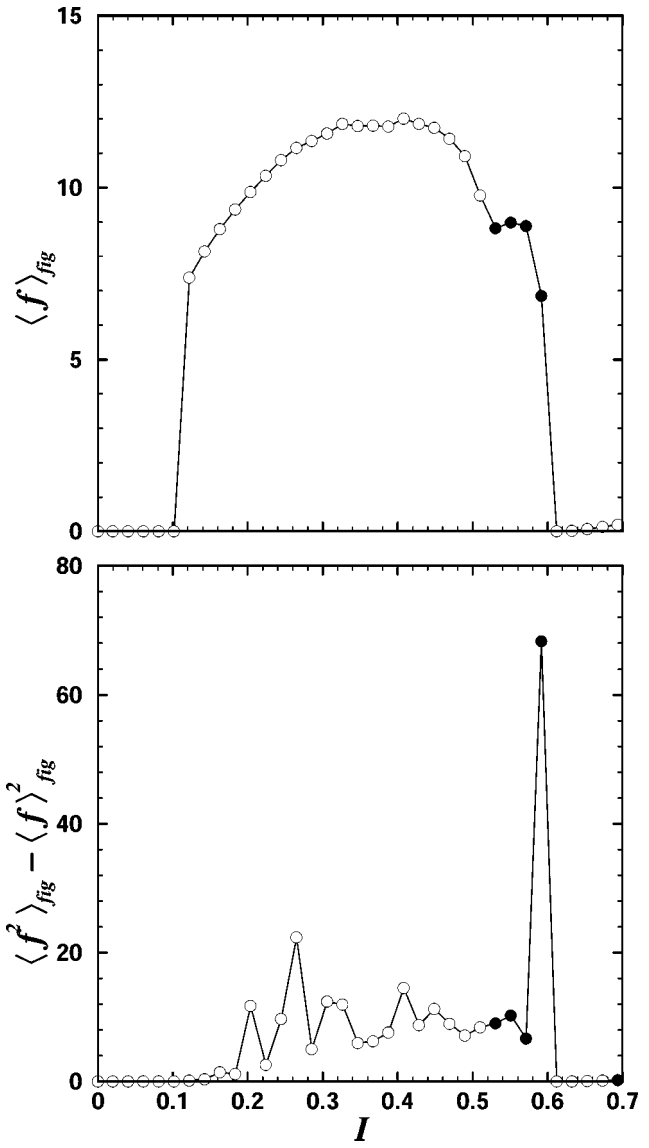

FIG. 4. Mean value of the oscillator frequency over the figure pixels, as a function of the input current for the FitzHugh-Nagumo system (top); fluctuations (bottom).

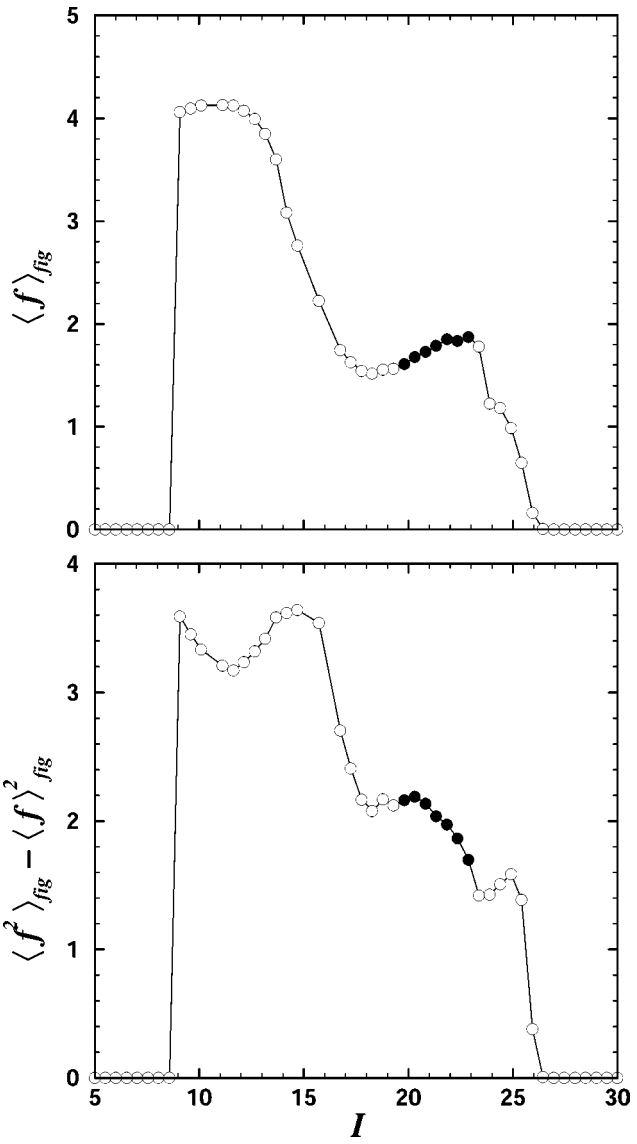

FIG. 5. Mean value of the oscillator frequency over the figure pixels, as a function of the input current for the Morris-Lecar system (top); fluctuations (bottom).

nal current takes 1 h in the same 300-MHz, Pentium II PC. It is important to note that this is possibly, in opposition to the spin system case, the smallest time needed to generate good images with this method. The curve of the mean frequency as a function of the external current is presented in Fig. 4. The ○ represent the data points and the ● the points at which the best figures were found.

In almost the same manner we have worked with Morris-Lecar oscillators. The external currents are fixed at the interval $5<I_{ext}<30$. At currents above 26 and below 8, the system is disordered and oscillators are mainly independent (paramagnetic phase). When the current is raised above 8, the system enters in a ferromagnetic phase. The superparamagnetic *plateau* is found about $18<I_{ext}<23$. Beyond 26 the system returns to the paramagnetic phase. The time for a simulation of 200 plus 1000 integration steps at 50 different values of the external current takes 3 h in the same equipment. The curve of the mean frequency as a function of the external current is presented in Fig. 5. The ○ represent the data points and the ● the points at which the best figures were found.

B. The specialist

There is no general method to decide which is the best figure from all the ones generated at different values of the simulation parameters. For the present case, we have developed the following strategy. Using Fig. 1 and a simple image manipulation software, we have *painted* Fig. 6, which can be considered an eye segmentation of Fig. 1. Figure 1 is an x-ray computerized tomography image of a damaged human brain. It presents five regions that can be visualized easily: background, skin, bone, brain, and damaged tissue. These

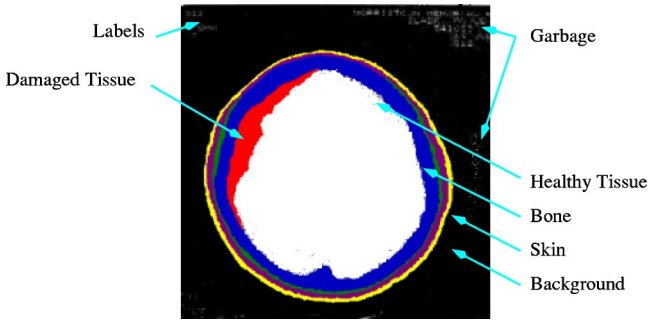

FIG. 6. Figure 1 was *painted* by hand to produce the present figure, which can be considered an eye segmentation. Figure 1 presents five regions that can be visualized with ease: the dark background, the skin, the bone, the brain, and the damaged tissue. These structures were preserved in the specialist. Labels and other structures (such as the bright strip at the right of the figure or the tiny bright structures at the top right) are not interesting for segmentation purposes and they were mainly deleted.

structures were preserved in the specialist. Labels and other structures are not interesting for segmentation purposes and they were mainly deleted from the specialist.

In order to compare the reference image with the simulated segmented images, we automatically estimate how many pixels in both images belong to similar clusters. We assign as correct, a pixel in the segmented image that belongs to a cluster comparable in size to the cluster of the pixel at the same position in the specialist figure. While this does not always ensure a faithful measure, it was found to be reasonable for the present case, where the principal segments are quite different in size. Let us consider M biggest clusters of areas $A_1, A_2, \ldots, A_M$ in the reference image, and associate to them M counters $N_1, N_2, \ldots, N_M$, set to zero. If the pixel at the position (x,y) in the reference image belongs to A_i and the pixel at the same position in the simulated figure belongs to a cluster of area $\tilde{A}$ such that $|A_i - \tilde{A}|/A_i < 0.5$, the counter N_i is increased in one. After comparing all the pixels, one by one, the following quantity is taken as a quality measure of the simulated image:

$$Q = \frac{1}{M} \sum_{i=1}^{M} \frac{N_i}{A_i}. \tag{11}$$

For different values of the threshold θ and the control parameter, the best images according to Q are those presented in Fig. 7 for the spin system, in Fig. 8 for the FitzHugh-Nagumo system, and in Fig. 9 for the Morris-Lecar system.

IV. CONCLUSIONS

We have used the idea of superparamagnetic clustering with neural units instead of the usual magnetic Potts spins. While artificial neurons have long been based on magnetic analogies, the dynamical properties are seldom well represented by Ising or Potts spins. Segmentation in the brain is performed to extract information about color, form, distance, or size. Several parallel pathways and areas are responsible for each type of feature extraction and presumably somehow

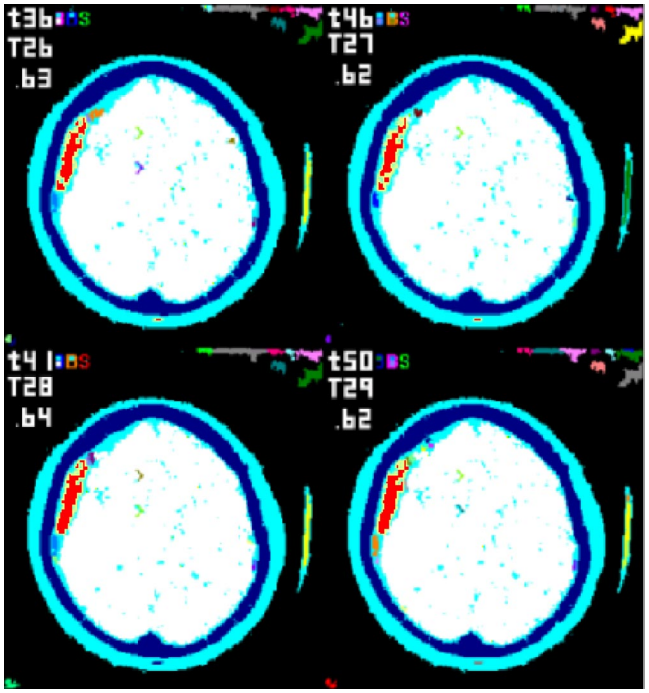

FIG. 7. Best simulated images according to Q, considering $M=10$, with $k_BT=0.098\,47\varepsilon$, $\theta=0.36$, and $Q=0.63$, $k_BT=0.094\,41\varepsilon$; $\theta=0.46$, and $Q=0.62$; $k_BT=0.090\,35\varepsilon$, $\theta=0.41$, and $Q=0.64$; and $k_BT=0.086\,29\varepsilon$, $\theta=0.50$, and $Q=0.62$, for the upper left, upper right, lower left, and lower right panels, respectively. The light gray (cyan for the on-line version of the paper) structure around the bone is noise.

these bind together to form the mental representation of the visual scene. The idea of synchronization or coherent oscillation for the feature extraction and binding is quite prominent in vision research. Although our model does not represent the neural architecture in a realistic way, it holds some elements which can permit thinking about visual segmentation in terms of analogous superparamagnetic clustering. The main ingredient in our neural segmentation model is that the coupling between the units is proportional to the difference in membrane potential times the coupling J_{ij}. It is here that the information from the image enters, and it can be thought as a lateral pathway arising from a connection mediated by interneurons that receive information from the receptor cells. Of course whether this occurs at a retinal level or further down is not addressed by our model. As described above, all the oscillators are stimulated by the same external current. Synchrony among similar oscillators is then achieved by the modulation action of the factor proportional to the difference of the membrane potential in Eq. (9).

The example presented here is just an illustration of the capabilities of the present method. The required time for an image segmentation can be shorter if the number of MC passes (MCPs) is reduced. The magnetization curve remains the same (within statistical errors) if the number of MCPs is reduced by a factor of 50. Therefore, in about 6 min it is possible to produce the magnetization curve (with bigger error bars but with clear information about the different phases) and images with the same quality as the ones pre-

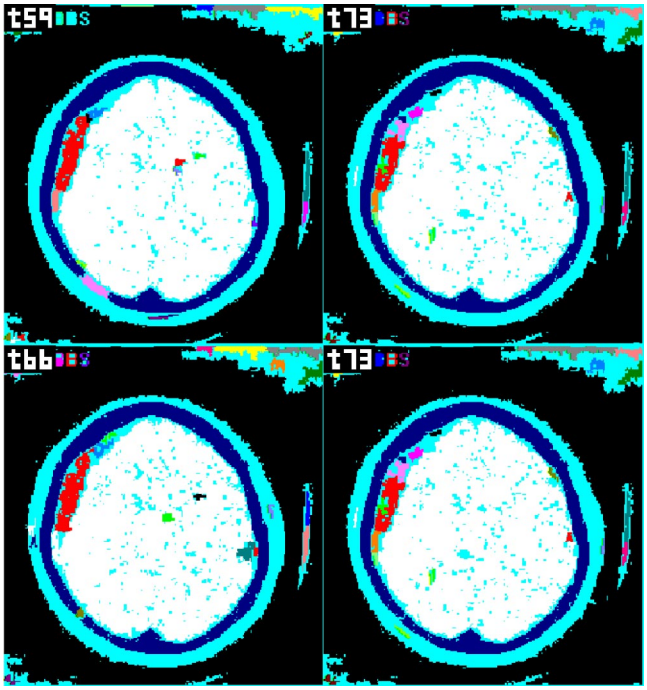

FIG. 8. Best segmentation figures for the FitzHugh-Nagumo oscillator system. The values of the input currents and thresholds are $I=0.59$ and $\theta=0.59$ for the upper left figure, $I=0.57$ and $\theta=0.73$ for the upper right figure, $I=0.55$ and $\theta=0.66$ for the lower left figure, and $I=0.55$ and $\theta=0.73$ for the lower right figure. The quality factors for all the figures are above 0.6. The light gray (cyan for the on-line version of the paper) structure around the bone is noise.

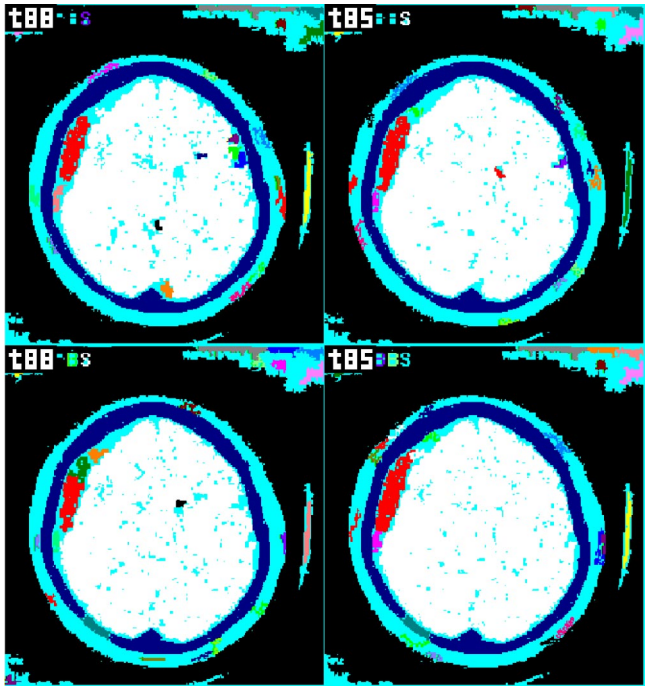

FIG. 9. Best segmentation figures for the Morris-Lecar oscillator system. The values of the input currents and thresholds are $I=21.84$ and $\theta=0.88$ for the upper left figure, $I=21.33$ and $\theta=0.85$ for the upper right figure, $I=20.31$ and $\theta=0.88$ for the lower left figure, and $I=19.80$ and $\theta=0.85$ for the lower right figure. The quality factors for all the figures are above 0.6. The light gray (cyan for the on-line version of the paper) structure around the bone is noise.

sented in Fig. 7. This time can be reduced in an order of magnitude by the use of the ECU algorithm [9,10], improving the applicability of this segmentation technique to problems such as the fast automatic calculation of segment areas from medical images. There are no important changes in the figure if the number M of clusters considered to calculate Q is increased. It is not obvious how to diminish the time used to perform the calculation with the oscillator systems. Nevertheless, the quality of the pictures found is the same as in the spin system. Inherent parallelism in a biological system leads, however, to a reduction of the computation times by a factor of the order of the number of units. From the point of view of the comparison with the specialist, the three methods are equivalent. Furthermore, for each of the methods the best parameters are the same if the specialist is substituted by the segmentation image of any one of the other two methods.

This model can be expanded in several ways, by putting in more layers and trying to include more realistic biological elements. This, however, was not our aim, as we tried to show that the important clustering ideas put forward by Domany and co-workers can find a parallel in natural systems, if not identical in the details, at least in spirit. Although Potts spins are not to be found in natural brains, the analogous superparamagnetic clustering can still be implemented using the available neurons.

ACKNOWLEDGMENTS

J.P.N. was supported by the FAPESP. J.P.N., S.M.K., and N.C. acknowledge the partial support from the CNPq.

[1] M. Blatt, S. Wiseman, and E. Domany, Phys. Rev. Lett. **76**, 3251 (1996); Neural Comput. **9**, 1805 (1997); S. Wiseman, M. Blatt, and E. Domany, Phys. Rev. E **57**, 3767 (1998).
[2] F.Y. Wu, Rev. Mod. Phys. **54**, 235 (1982).
[3] H. Wersing, J.J. Steil, and H. Ritter, Neural Comput. **13**, 357 (2001).
[4] D. Wang and D. Terman, Neural Comput. **9**, 805 (1997).
[5] D. Wang and D. Terman, IEEE Trans. Neural Netw. **6**, 283 (1995).
[6] A. Labbi, R. Milanese, and H. Bosch, in *Proceedings of International Workshop on Artificial and Natural Neural Networks (IWANN '97), Lanzarote*, edited by J. Mira, R. Moreno Díaz, and J. Cabestany (Springer-Verlag, Berlin, 1997).
[7] A. Labbi, R. Milanese, and H. Bosch, in *Proceedings of International Symposium on Nonlinear Theory and Applications (NOLTA '97), Hawaii* (IEICE, Tokyo, 1997), p. 581.
[8] S. Wang and R.H. Swendsen, Physica A **197**, 565 (1990).
[9] R. Opara and F. Wörgötter, Neural Comput. **10**, 1547 (1998).

[10] C. von Ferber and F. Wörgötter, Phys. Rev. E **62**, R1461 (2000).
[11] A.L. Hodgkin and A.F. Huxley, J. Physiol. (London) **117**, 500 (1952).
[12] C. Koch, *Biophysics of Computations: Information Processing in Single Neurons* (Oxford University Press, New York, 1999).
[13] R. FitzHugh, Biophys. J. **2**, 11 (1961).
[14] J.S. Nagumo, S. Arimoto, and S. Yoshizawa, Proc. IRE **50**, 2061 (1962).
[15] C. Morris and H. Lecar, Biophys. J. **193**, 193 (1981).
[16] J. Rinzel and B.B. Ermentrout, in *Methods of Neuronal Modeling*, edited by C. Koch and I. Segev, 2nd ed. (MIT Press, Cambridge, MA, 1998).
[17] J.M. Bower and D. Beeman, *The Book of Genesis*, 2nd ed. (Springer-Verlag, New York, 1997), p. 334.